 CMES, vol.55, no.1, pp.33-60, 2010

Numerical Characterization of Porous Solids and Performance Evaluation of Theoretical Models via the Precorrected-FFT Accelerated BEM

Z. Y. Yan[1,2], J. Zhang[1], W. Ye[1] and T.X. Yu[1]

Abstract: An 3-D precorrected-FFT accelerated BEM approach for the linear elastic analysis of porous solids with randomly distributed pores of arbitrary shape and size is described in this paper. Both the upper bound and the lower bound of elastic properties of solids with spherical pores are obtained using the developed fast BEM code. Effects of porosity and pore shape on the elastic properties are investigated. The performance of several theoretical models is evaluated by comparing the theoretical predictions with the numerical results. It is found that for porous solids with spherical pores, the performances of the generalized self-consistent method and Mori-Tanaka method are comparable and are much better than that of the self-consistent method and the differential scheme. In particular, the generalized self-consistent method gives the best approximations to three elastic moduli while Mori-Tanaka method agrees particularly well with the numerical value of Poisson's ratio.

Keywords: Boundary element method, pFFT acceleration technique, porous material, elastostatics, random distribution

1 Introduction

Porous materials are an important class of materials that have been widely utilized in a variety of fields. Mechanical characterization is without doubt an essential step in the applications of these materials. Over the past fifty years, many theoretical approaches have been proposed for the evaluation of the effective elastic mechanical properties of composite/porous materials. These approaches are however based on various simplifications. For example, the self-consistent method calculates the effective properties by assuming that any inclusion/void is surrounded by the effective as-yet-unknown material [Budiansky (1965); Hashin (1962); Hill (1965)].

[1] Department of Mechanical Engineering, Hong Kong University of Science and Technology
[2] Department of Aerodynamics, Nanjing University of Aeronautics and Astronautics

The differential scheme (DS) proposed by Norris was derived based on the idea of realization; that is, the composite is assumed to be formed by adding inclusions of different phases to the current matrix iteratively until the inclusions reach the required volume fraction [Norris (1985)]. The generalized self-consistent method (GSCM) [Benveniste (2008); Christensen (1998); Christensen and Lo (1979); Lu, Huang and Wang (1995)] supposes that the inclusion is coated by a matrix material shell and then is wholly embedded in the effective as-yet-unknown material. Based on the framework of the "direct approach", Benventiste (1987) elucidated that the essential approximation in Mori-Tanaka's method [Mori and Tanaka (1973); Benveniste (1987); Hwang and Huang (1999)] was that the concentration factors were found by embedding a single particle in an all-matrix medium subject to a uniform stress or strain at infinity. Unlike the simple model based on the "dilute" approximation, the applied uniform stress or strain was the average stress or strain of the matrix. As such, the interactions between inclusions were accounted for. A common and essential requirement in all the above schemes is that the material has to be macroscopically isotropic and homogeneous. This is however difficult to be met in practice because many porous materials particularly those naturally formed such as bone are inherently heterogeneous.

With the advent of advanced numerical techniques and rapidly developed computing power, detailed three-dimension numerical modeling of realistic porous solids has become increasingly popular due to its capability to produce accurate predictions of mechanical responses of these structures and its capability of capturing the effects of non-uniform distribution, irregular shapes and size on the overall behavior of porous solids. Such a trend can be clearly observed from the literature where the recent modeling effort has been shifted from analytical analysis towards numerical simulations. Examples include but are not limited to Day, Snyder, Garboczi and Thorpe (1992); Gusev (1997); Simone and Gibson (1998); Hu, Wang, Tan, Yao and Yuan (2000); Roberts and Garboczi (2000); Segurado and Llorca (2002); Segurado, Gonzalez and Llorca (2003); Yao, Kong and Zheng (2003); Gatt, Monerie, Laux and Baron (2005) and Kari, Berger, Rodriguez-Ramos and Gabbert (2007).

It is perhaps fair to say that the current leading method in the simulation of porous solids is the finite element method (FEM). Indeed, the FEM is a mature, powerful and versatile method suitable for an extremely wide scope of problems. However, one challenge in using the FEM is the generation of good-quality volume fitting mesh for problems with complex 3-D domains. With irregular shapes and random distribution of pores, porous solids particularly those with large porosity could be one of these examples in which a good quality volume mesh is difficult to produce. The boundary element method (BEM) [Banerjee (1994)], on the other hand, requires only surface mesh for linear problems. It is thus particularly suitable for

problems with complex 3-D geometry and/or moving boundaries. Applications of the BEM can be found in many fields including, for example, stress analysis [Tan, Shiah and Lin (2009)], crack propagation [Karlis, Tsinopoulos, Polyzos and Beskos (2008)], contact problems [Zozulya (2009)], analysis of graded isotropic elastic solids [Criado, Ortiz, Mantič, Gray and París (2007)], elastoplastic problems [Owatsiriwong, Phansri and Park (2008)], electromagnetics [Soares and Vinagre (2008)], acoustics [Yan, Hung and Zheng (2003); Yang (2004)] and fluid mechanics [Mantia and Dabnichki (2008)]. For porous solids, the surface mesh of each pore and the solid phase can be generated independently and parallel, greatly reducing the meshing complexity and improving the meshing efficiency. In addition, the recently developed acceleration techniques, such as the fast multipole method (FMM) [Greengard and Rokhlin (1997)], the precorrected Fast Fourier Transformation (pFFT) technique [Phillips and White (1997)], the combined fast Fourier transform and multipole method [Ong, Lim, Lee and Lee (2003)], the panel clustering method [Hackbusch and Nowak (1989); Aimi, Diligenti, Lunardini and Salvadori (2003)], and the adaptive cross approximation technique [Bebendorf, Rjasanow (2003); Brancati, Aliabadi and Benedetti, (2009)] when combined with the iterative linear system solvers, have greatly reduced the computational time and the memory required in solving the discretized system, making the BEM suitable for large-scale problems. Successful applications of the accelerated BEM in solving large scale problems can be found in the areas of microelectromechanical systems [Ye, Wang, Hemmert, Freeman and White (2003); Ding and Ye (2004); Frangi and Gioia (2005)], composite materials [He, Lim and Lim (2008); Liu, Nishimura and Otani (2005); Liu, Nishimura, Otani, Takahashi, Chen and Munakata (2005); Wang and Yao (2005); Wang and Yao (2008); Wang and Yu (2008)], graphite materials [Wang, Hall, Yu and Yao (2008)], corrosion problems [Aoki , Amaya, Urago and Nakayama (2004)], electromagnetics [Chew, Song, Cui, Velamparambil, Hastriter and Hu (2004)], etc. In the applications related to mechanical analysis of porous solids, Liu presented a FMM accelerated BEM for the elastostatic analysis of 2D structures and analyzed the perforated plates with many uniformly or randomly distributed holes [Liu (2006)]. Wang and Yu (2008) studied the mechanical and thermal properties of three dimensional nuclear graphite with several hundred randomly distributed micro pores using the FMM accelerated BEM. He, Lim and Lim (2008) employed the fast Fourier transform on multipole method to study the elastic properties of porous materials with uniformly distributed voids.

In this paper, an efficient boundary element method based on the precorrected Fast Fourier Transformation (pFFT) technique is developed for the linear elastostatic analysis of 3-D porous solids with randomly distributed pores of arbitrary shapes. This method is then employed to numerically study the effective elastic properties

of solids with ellipsoidal pores of various porosities. The effects of some important parameters such as the pore shape and size are numerically investigated. In addition, the performance of some theoretical models is evaluated via the comparison between the numerical results and theoretical predictions. In the following section, methods for the generation of geometric models of porous solids with randomly distributed pores are described. It is followed by a description of the boundary integral formulation for elastostatics and the pFFT technique. Some important issues in the numerical implementation such as the evaluation of nearly singular and singular integrals are also discussed. Next elastic properties deduced from several theoretical approaches are presented. In Section 5, validation of the developed method and code is described followed by the presentation of the mechanical characterization of various porous solids and the comparison with various theoretical models. A summary of the presented work is given in Section 7.

2 Model generation of porous solids

To facilitate the comparison with theoretical models, cubes with randomly but macroscopically homogeneously distributed spherical pores of different porosities are constructed and employed to study the relationship between the effective elastic properties and the porosity. Two common algorithms for the generation of randomly distributed non-overlap spherical pores are the random sequential addition algorithm (RSA) and the Gusev scheme [Gusev (1997); Rintoul and Torquato (1997)]. In the RSA, pores are added sequentially at locations that are randomly selected. This method is easy to implement, but the porosity it can generate can not exceed 0.3. Modifications or other schemes should be devised if a larger porosity is desired [Kari, Berger, Rodriguez-Ramos and Gabbert (2007); Segurado and Llorca (2002)]. In the Gusev scheme, spherical pores are generated initially on a cubic lattice. They are then allowed to move sequentially about a certain distance along a randomly chosen direction if the following conditions are met: (1) the distance between the pore to be relocated and any other pores is larger than or equal to $2r+\delta$, where r is the radius of the spherical pore and δ is a positive value, and (2) the distance from this pore to the boundary of the cube is larger than or equal to $r+\delta$. In this work, δ is chosen to be $0.05r$ and the distance that each pore moves is a random value uniformly distributed in the range of $(0,d)$, where d is the initial gap between two pores. The movement continues until a macroscopically homogeneous model is obtained. Based on our experience, it is easier to generate models with high porosities using the Gusev scheme. Hence this scheme is employed for the generation of models with high porosity.

The inhomogeneous level of the pore distribution is accessed using the pair correlation function defined as $g(1)=\frac{V}{4\pi r^2 N}\frac{dK(l)}{dl}$, where $K(1)$ is the average number of

spherical pores located within a distance, l, from any sphere and N represents the total number of pores in the volume V considered [Segurado and Llorca (2002)]. In a statistically homogeneous distribution, the correlation function should approach to one as l increases. Fig.1 shows the pair correlation function of a model obtained after two million movement steps as a function of the ratio of l and r. From this plot, it is evident that the distribution of the spherical pores is statistically homogeneous.

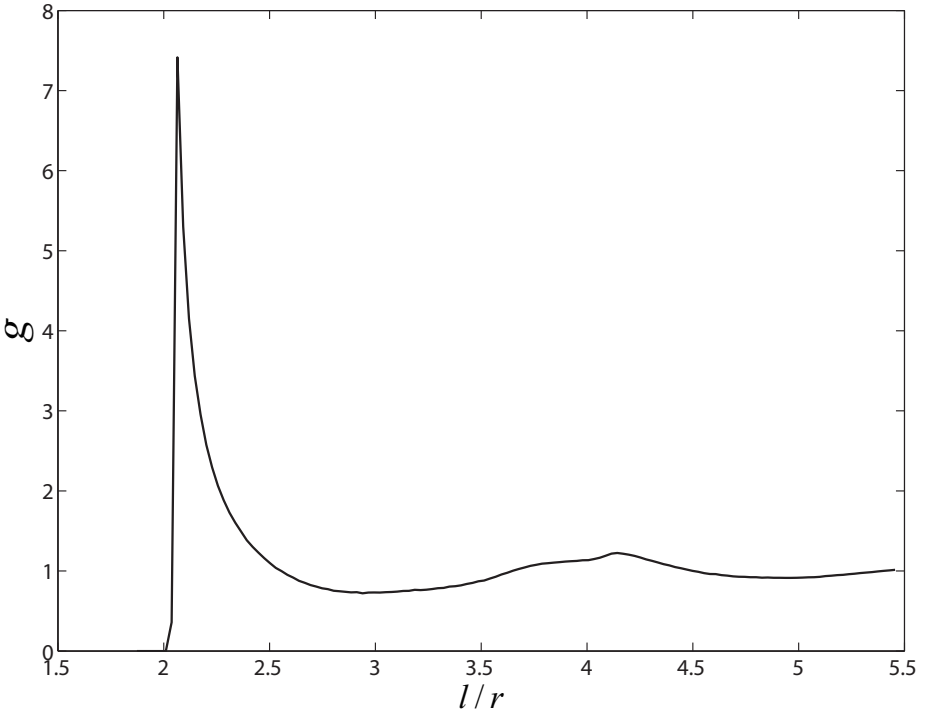

Figure 1: Pair correlation function of a model containing 125 spherical pores with a volume porosity of 0.4.

In this work, the influence of pore shape on the mechanical response of porous solids is also studied. Hence, models with non-overlapping ellipsoidal pores of different shapes are generated and the RSA algorithm is employed for the generation. In the implementation of the RSA algorithm, the most critical step is the detection of the overlap between two pores. For ellipsoids, a method proposed by Wang, Wang and Kim (2001) is employed. The generation procedure is as follows: an ellipsoid with its centroid located at (x_o, y_o, z_o) and its three semi-principal axes along

the three randomly chosen but uniformly distributed and mutually perpendicular directions is generated first. A check for any overlap with the existing pores or the outer surfaces of the solid is then performed. If none has been detected, this ellipsoid is kept. Otherwise it is deleted and a new ellipsoid is generated following the same procedure. The aforementioned detection method however does not exclude the contacting cases. To guarantee a minimum distance between the pores, ellipsoids are shrunk about 2.5% of their initial size. Fig.2 shows the interior of three models with randomly distributed ellipsoidal pores of different aspect ratios. The volume porosity in all three models is $c = 0.2$.

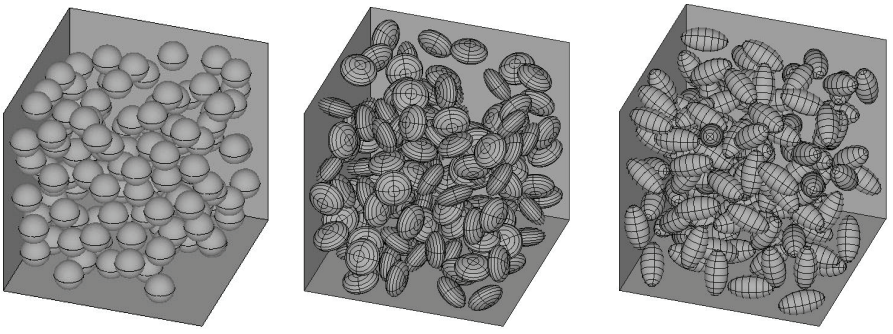

(a) $\lambda = 1.0$ (spherical pores) (b) $\lambda = 0.5$ (c) $\lambda = 2.0$

Figure 2: Three models of a cube with ellipsoidal pores of different aspect ratio, λ defined as the ratio of two radii.

3 The precorrected-FFT accelerated boundary element method for elastostatics

3.1 Boundary integral formulation for elastostatics

Consider a 3D linear elastostatic interior problem. In the absence of body forces, the integral formulation of the Navier's equation reads [Banerjee (1994); Becker (1992)]

$$c_{ij}(p)\,u_j(p) = \iint_S [G_{ij}(p,q)\,\tau_j(q) - F_{ij}(p,q)\,u_j(q)]dS_q, \tag{1}$$

where the kernels $G_{ij}(p,q)$ and $F_{ij}(p,q)$ are given as

$$G_{ij}(p,q) = \frac{C_1}{r}\left(C_3\delta_{ij} + \frac{\partial r}{\partial x_i}\frac{\partial r}{\partial x_j}\right) \tag{2}$$

and

$$F_{ij}(p,q) = -\frac{C_2}{r^2}\left\{\frac{\partial r}{\partial n_q}\left(C_4\delta_{ij} + 3\frac{\partial r}{\partial x_i}\frac{\partial r}{\partial x_j}\right) + C_4\left(n_i\frac{\partial r}{\partial x_j} - n_j\frac{\partial r}{\partial x_i}\right)\right\}. \tag{3}$$

In the above equations, $\mathbf{n} = [n_1\ n_2\ n_3]^T$ represents the outward unit normal vector, $r(p,q)$ represents the Euclidean distance between points p and q, and δ_{ij} is the Kronecker delta function. On smooth boundaries, the solid angle $c_{ij}(p) = 0.5\delta_{ij}$. It is δ_{ij} when p is inside the domain and 0 when p is outside the domain. The subscripts i and j in the above equations denote the index of the degrees of freedom and the Einstein summation convention is implied. The constants C_1, C_2, C_3, C_4 in Eqs. (2) and (3) are $C_1 = \frac{1}{16\pi G(1-\nu)}$, $C_2 = \frac{1}{8\pi(1-\nu)}$, $C_3 = 3-4\nu$, $C_4 = 1-2\nu$ respectively, where $G = \frac{E}{2(1+\nu)}$ is the shear modulus, E is the Young's modulus and ν is the Poisson's ratio.

Stress σ_{ij} inside the structure can be expressed in terms of the boundary quantities as

$$\sigma_{ij}(p) = \iint_S \left[G^{\sigma}_{kij}(p,q)\,\tau_k(q) - F^{\sigma}_{kij}(p,q)\,u_k(q)\right] dS_q, \tag{4}$$

where the kernels G^{σ}_{kij} and F^{σ}_{kij} are given by

$$G^{\sigma}_{kij}(p,q) = \frac{C_2}{r^2}\left\{C_4\left(\delta_{ki}\frac{\partial r}{\partial x_j} + \delta_{kj}\frac{\partial r}{\partial x_i} - \delta_{ij}\frac{\partial r}{\partial x_k}\right) + 3\frac{\partial r}{\partial x_i}\frac{\partial r}{\partial x_j}\frac{\partial r}{\partial x_k}\right\} \tag{5}$$

$$\begin{aligned} F^{\sigma}_{kij}(p,q) = &-\frac{2\mu C_2}{r^3}\left\{n_i\left[3\nu\frac{\partial r}{\partial x_j}\frac{\partial r}{\partial x_k} + C_4\delta_{jk}\right] + n_j\left[3\nu\frac{\partial r}{\partial x_i}\frac{\partial r}{\partial x_k} + C_4\delta_{ik}\right] + \right. \\ &n_k\left[3C_4\frac{\partial r}{\partial x_i}\frac{\partial r}{\partial x_j} + (1-4\nu)\,\delta_{ij}\right] \\ &\left. + 3\frac{\partial r}{\partial n_q}\left(C_4\delta_{ij}\frac{\partial r}{\partial x_k} + \nu\left(\delta_{jk}\frac{\partial r}{\partial x_i} + \delta_{ik}\frac{\partial r}{\partial x_j}\right) - 5\frac{\partial r}{\partial x_i}\frac{\partial r}{\partial x_j}\frac{\partial r}{\partial x_k}\right)\right\}. \end{aligned} \tag{6}$$

3.2 The precorrected-FFT algorithm for elastostatics

In the conventional BEM, the final influence matrices are dense. This feature has greatly limited the application scope of the BEM in the modeling of large-scale problems. Fortunately, several acceleration algorithms have been invented in the past several decades. The combination of the fast algorithms and iterative solvers has greatly reduced both the memory usage and the computational time required. One of the popular acceleration schemes is the precorrected-FFT technique [Phillips and White (1997)]. This scheme is easy to implement and has the

advantage of being relatively kernel independent. Similar to the other acceleration schemes such as the fast multipole method, the main idea of the precorrected-FFT acceleration scheme is that instead of computing the influence matrix entries corresponding to the far-field interaction explicitly and then multiplying them with the sources, the far-field interactions are computed directly via an approximate method. More specifically, in the precorrected-FFT (pFFT) technique, a parallelepiped is constructed to enclose a three-dimensional problem after it has been discretized into n surface panels. This parallelepiped is then subdivided into an array of small cubes so that each small cube contains only a few panels. Fig. 3(a) shows a 2-D view of a quarter of a discretized 3-D solid block with a spherical cavity located at its center. The parallelepiped which has been divided into an $7 \times 7 \times 7$ array of small cubes is shown in Fig. 3(b) together with the discretized block. It should be pointed out that the surface panels and the pFFT cubes can intersect with each other. There is no need to maintain any consistency between the surface panels and the cubes. The acceleration of surface integration is achieved by exploiting the fact that the kernels in the surface integrals such as those in Eqs. (2) and (3) have piecewise-smooth convolution form. Thus with the aid of the uniform grid formed by the cubes in the parallelepiped, these integrals can be computed approximately using the Fast Fourier Transform technique. To ensure accuracy, such an approximation is only employed for far-field interactions, that is, integrals in which the evaluation point is far away from the field panel (Figure 3(c)). For nearby interactions, direct evaluation is required. The main steps in the precorrected-FFT acceleration technique include

(1) Construction and superposition of the 3-D uniform grid and the discretized problem domain (Fig. 3(b));

(2) Determination of the near- and far-field for each panel using the cubes of the parallelepiped; for example, for panel P inside cube S, its near field and far field are illustrated in Fig. 3 (c);

(3) Projection of the panel source onto the surrounding grid points based on polynomial interpolation;

(4) Calculation of the grid to grid integration using the Fast Fourier Transformation;

(5) Interpolation of the grid interaction back to panels;

(6) Subtraction of the near-field interaction;

(7) Computation of the near-field interaction using direct calculation;

(8) Summation of the near-field and far-field contributions.

For a detailed description of this technique, readers are referred to Phillips and White (1997) and Masters and Ye (2004).

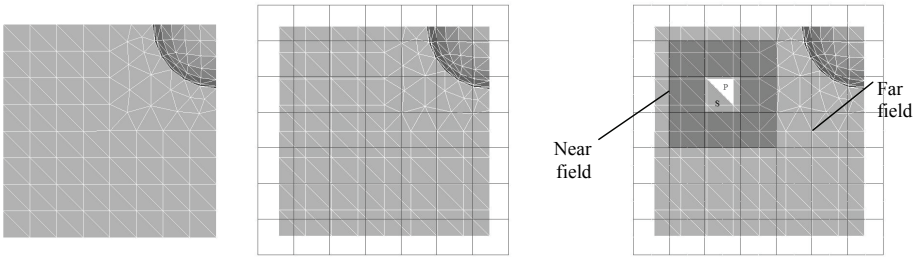

(a) (b) (c)

Figure 3: Side views of a problem domain: one quarter of a solid block with a spherical cavity located at its center: (a) surface mesh of the problem domain (852 panels); (b) the superimposed 3-D parallelepiped decomposed into $7 \times 7 \times 7$ cubes and the surface mesh; (c) illustration of the near field and far field of panel P located inside cube S.

3.3 Numerical implementation

A piecewise constant collocation scheme is employed to discretize the integral equation shown in Eq. (1). The surfaces of the solid and each pore are discretized into small triangular panels. At each panel, the displacement and the traction are assumed to be constant. The resultant linear system is then solved using the generalized minimal residual algorithm (GMRES) [Saad and Schultz (1986)] accelerated with the precorrected-FFT technique.

A major challenge in the solution procedure is the accurate evaluation of the nearly singular and singular integrals which occur quite frequently in porous solids particularly when the porosity is large. In the literature, a variety of methods have been proposed and developed for the evaluation of nearly singular integrals [Scuderi (2008); Ye (2008)], weakly singular integrals [Han and Atluri (2007); Nagarajan and Mukherjee (1993)], strongly singular [Cruse (1969); Ding and Ye (2004); Liu (2000)] and hypersingular integrals [Chen and Hong (1999); Dominguez, Ariza and Gallego (2000); Gao, Yang and Wang (2008); Li, Wu and Yu (2009); Qian, Han and Atluri (2004); Qian, Han, Ufimtsev and Atluri (2004); Sanz, Solis and Dominguez (2007); Yan, Cui and Hung (2005)]. In this work, the nonlinear transformation technique described by Ye (2008) is employed to compute the nearly

singular integrals. The weakly singular integrals associated with the G kernel (Eq. (2)) are evaluated using the method proposed by Nargarjan and Mukherjee (1993) in which a transformation to the polar coordinate system is employed to eliminate the near singularity. For the evaluation of strongly singular integrals; that is, those associated with the F kernel, the analytical method proposed by Cruse (1969) is employed. In this method, each triangular panel is first divided into three subtriangles with the centroid of the origin panel being the common vertex as illustrated in Fig. 4. A local coordinate system with the origin at the centroid is then set up for each subtriangle. For example, for the subtriangle $c20$, a local coordinate system $\xi_1\xi_2$ is constructed so that the axis ξ_1 is parallel to the edge and the axis ξ_2 is perpendicular to the edge. The integration of the kernel $C_2C_4\frac{1}{r^2}\left(n_i\frac{\partial r}{\partial x_j}-n_j\frac{\partial r}{\partial x_i}\right)$ on this subtriangle can then be obtained analytically as

$$I_{ij}^{c20}=-C_2C_4\varepsilon_{ijk}e_{1k}\left[\log\left(\xi_1+r\right)\right]_0^2, \tag{7}$$

where ε_{ijk} is the permutation tensor, e_{1k} is the projection of the unit vector of along ξ_1-axis on the k-th global axis, and the variable r represents the distance between a point on the edge and the centroid of the original panel c.

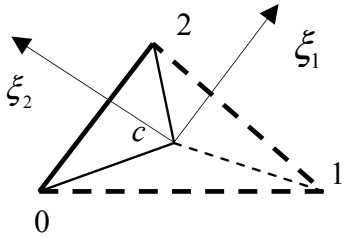

Figure 4: Illustration of the local coordinate system of the subtriangle $c20$.

It should be noted that due to flat panels, the integral corresponding to the first term in the F kernel (Eqn. (3)) vanishes because $\partial r/\partial n_q \equiv 0$.

4 Theoretical models

Several theoretical schemes are employed to calculate the effective elastic properties of porous materials with spherical pores. These properties are used in the performance comparison presented in Section 5. Throughout the rest of the paper, the effective shear, bulk, Young's moduli and Poisson's ratio are denoted as G, K, E and v, respectively. Letters with subscript m represent material properties of the matrix.

4.1 Self-consistent method

By setting both the shear and bulk moduli of inclusions to be zero in Eqs. (2-6)-(2-10) in Budiansky (1965), the effective shear and bulk moduli of porous materials with spherical pores satisfy the following two equations:

$$\frac{1}{G} = \frac{1}{G_m} + \frac{c}{(1-\beta)G} \tag{8}$$

$$\frac{1}{K} = \frac{1}{K_m} + \frac{c}{(1-\alpha)K}, \tag{9}$$

where $\alpha = \frac{1+\nu}{3(1-\nu)} = \frac{3K}{3K+4G}$,$\beta = \frac{2(4-5\nu)}{15(1-\nu)} = \frac{6(K+2G)}{5(3K+4G)}$. Further mathematic manipulation yields the following equations from which the effective shear and bulk moduli can be readily obtained.

$$8G^2 + [3(3-c)K_m - 8G_m + 20 \cdot c \cdot G_m]G + (18c-9)K_m G_m = 0, \tag{10}$$

$$K = \frac{4(1-c)K_m G}{4G + 3cK_m} \tag{11}$$

4.2 Differential scheme

Based on the idea of realization, the expressions [Norris (1985)] for the effective bulk and shear moduli of porous materials in the differential form are obtained as,

$$\frac{dK}{dc} = -K\frac{3K+4G}{4G}\frac{1}{1-c} \tag{12}$$

$$\frac{dG}{dc} = -G\frac{15K+20G}{9K+8G}\frac{1}{1-c} \tag{13}$$

with the initial conditions of $K(0) = K_m$ and $G(0) = G_m$. Using the central difference method one can obtain the numerical values of K and G from Eqs. (12) and (13).

4.3 Generalized self-consistent method

In this method, the inclusions/pores are coated with a matrix shell and then are embedded in an infinite effective material with as-yet-unknown elastic constants [Benveniste (2008); Christensen and Lo (1979)]. Formulas for the effective properties of porous materials can be derived and are given as,

$$\frac{K}{K_m} = 4\frac{(1-c)G_m}{4G_m + 3cK_m} \tag{14}$$

$$A(\frac{G}{G_m})^2+2B\frac{G}{G_m}+C=0 \tag{15}$$

where

$$A=4(7-10v_m)(7-5v_m)+50(7-12v_m+8v_m^2)c-252c^{5/3}+25(7-v_m^2)c^{7/3} \\ +2(4-5v_m)(7+5v_m)c^{10/3},$$

$$B=-(3/2)(7-5v_m)(7-15v_m)-75v_m(3-v_m)c+252c^{5/3}-25(7-v_m^2)c^{7/3} \\ +(1/2)(7+5v_m)(5v_m-1)c^{10/3},$$

$$C=-(7-5v_m)(7+5v_m)+25(7-v_m^2)c-252c^{5/3}+25(7-v_m^2)c^{7/3} \\ -(7+5v_m)(7-5v_m)c^{10/3}.$$

For more detailed information please refer to Eqs.(3.15-3.18) in [Christensen and Lo (1979)] or Eqs.(31-33) in [Lu, Huang and Wang (1995)].

4.4 Mori-Tanaka method

The elastic moduli of porous materials can be obtained from Benveniste (1987) as,

$$\frac{K}{K_m}=4\frac{(1-c)G_m}{4G_m+3cK_m} \tag{16}$$

$$\frac{G}{G_m}=1-\frac{5(3K_m+4G_m)}{3(3+2c)K_m+4(2+3c)G_m}c \tag{17}$$

4.5 Hashin bounds

Based on the "variational principle", Hashin *et al* [Hashin (1962) ; Hashin and Shtrikman (1963)] derived the upper and lower bounds for both bulk and shear moduli of composite materials. When the inclusions/pores are spherical, the bounds of the bulk modulus coincide which yield the exact solution for the bulk modulus as shown in Eqn. (18).

$$\frac{K}{K_m}=4\frac{(1-c)G_m}{4G_m+3cK_m} \tag{18}$$

This formula is identical to that obtained from the generalized self-consistent method and Mori-Tanaka method shown in Eqs. (14) and (16). Unfortunately the bounds for the shear modulus do not coincide. Hashin (1962) provided a simple formula which produces an intermediate value between the two bounds.

$$\frac{G}{G_m}=1-\frac{5(3K_m+4G_m)}{3(3+2c)K_m+4(2+3c)G_m}c \tag{19}$$

5 Validation of the pFFT accelerated BEM

In this section, numerical simulations of two examples using the developed pFFT accelerated BEM code are presented. Results are compared with the analytical solution and the solution obtained from ANSYS, a commercial FEM software.

5.1 A pressurized thick-wall cylindrical vessel

A 3D pressurized thick-wall cylindrical vessel with an inner radius of $r_i = 3m$ and an outer radius of $r_o = 6m$ is subject to an inner pressure of $p_i = 1Pa$ and a zero outer pressure. The Young's modulus and the Poisson's ratio of the vessel material are $E_m = 1.0 \times 10^5 Pa$ and $\nu_m = 0.3$, respectively. The radial displacement of the vessel as a function of the radial distance r can be derived analytically as [Becker (1992); Lu and Luo (1997)]

$$u_r(r) = c_1 r + \frac{c_2}{r} \tag{20}$$

where $c_1 = \frac{1}{E^*}\frac{(1-\nu^*)r_i^2 p_i}{r_o^2 - r_i^2}$, $c_2 = \frac{1}{E^*}\frac{(1+\nu^*)r_i^2 r_o^2 p_i}{r_o^2 - r_i^2}$ and $E^* = \frac{E_m}{1-\nu_m^2}, \nu^* = \frac{\nu_m}{1-\nu_m}$.
Substituting the parameters associated with the vessel into Eqn. (20), one obtains $c_1 = 26/15 \times 10^{-6} \approx 1.73333 \times 10^{-6}$ and $c_2 = 1.56 \times 10^{-5} m^2$. Therefore, the analytical solutions of the radial displacements of the inner and outer cylindrical surfaces are $u_r(3)$ =57.2 μm and $u_r(6)$ =36.4 μm, respectively.

The developed 3-D pFFT accelerated BEM code is employed to calculate the radial displacement of the pressurized vessel. Due to symmetry, only a quarter of the structure is modeled. Fig. 5 shows the simulation domain together with its two discretized models. The height of the simulation model is set to be $H = 9m$. In order to model the infinitely long cylinder, symmetrical boundary conditions are applied at the top and the bottom surfaces. The simulated radial displacements at the inner and outer surfaces are listed in Table 1. Several different discretizations are employed starting from the coarse mesh with 60 triangular panels to the finest mesh with 59392 panels. The mesh is refined in such a way that the number of the elements along the edges of the structure is doubled in each refinement. Results obtained from the direct BEM simulations, i.e., without the acceleration, are also presented in Table 1 for comparison. Due to the limited memory of our computer, the finest discretization that can be simulated in the direct calculation is 3712. Overall, the linear convergence rate is observed in both sets of the results. In addition, the accuracies of the two sets of results are also comparable, indicating that the acceleration via the pFFT technique does not affect both the convergence rate and the accuracy. Also listed in Table 1 are the consumed memory and the CPU time associated with each method. To provide a clear picture of both the memory and

the CPU time, Fig. 6 plots the consumed memory and the CPU time as functions of the number of panels. The lines corresponding to $O(n)$, $O(n\log n)$ and $O\left(n^2\right)$ are also plotted for reference. It is evident that both the CPU time and memory usage of the pFFT accelerated BEM are of $O(n\log n)$, a great improvement from $O\left(n^2\right)$ particularly when n is large.

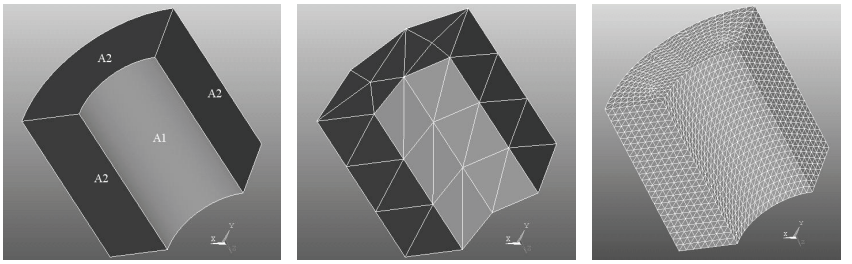

(a) One quarter of the vessel (b) Discretization with 60 panels (c) Discretization with 3712 panels

Figure 5: Simulation model and surface mesh for a pressurized thick-wall cylindrical vessel.

Table 1: Illustration of the convergence and efficiency of the pFFT BEM and the direct BEM

Method		Number of panels					
		60	232	928	3712	14848	59392
pFFT BEM	memory (MB)	3	21	51	174	1445	6509
	time (s)	2	11	36	156	1408	8719
	$u_r^o(\mu m)$	37.6250	36.7542	36.5204	36.5133	36.5062	36.4423
	error	3.37%	0.97%	0.33%	0.31%	0.29%	0.12%
	$u_r^i(\mu m)$	62.6100	59.0800	57.9006	57.6281	57.4708	57.3066
	error	9.46%	3.29%	1.22%	0.75%	0.47%	0.19%
Direct BEM	memory (MB)	3	23	266	4251		
	time (s)	2	14	228	4986		
	$u_r^o(\mu m)$	37.6250	36.7542	36.5742	36.4971		
	error	3.37%	0.97%	0.48%	0.27%		
	$u_r^i(\mu m)$	62.6100	59.0800	58.0275	57.6000		
	error	9.46%	3.29%	1.45%	0.70%		

5.2 A pressurized cube with a spherical cavity at its center

To further validate the in-house code based on the fast pFFT BEM for elastostatic problems, the case of a cube with a spherical cavity located at its center is simulated. Again the material is characterized by Young's modulus $E_m = 1.65 \times 10^5 Pa$

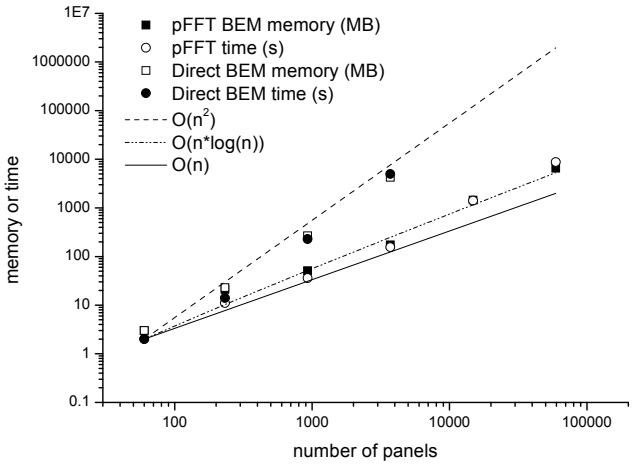

Figure 6: Consumed memory and computational time as functions of the number of panels

and Poisson's ratio $\nu_m = 0.33$. The length of the cube is set to be 1 m and the radius of the spherical cavity is 0.15 m. Uniform normal pressure $P = 1$ Pa is applied at the surfaces of $z = \pm 0.5$. Because of symmetry, only one octant of the cube is modeled as shown in Fig. 7. The boundary conditions of the simulation model are that the normal pressure of 1 Pa is set at $z = 0.5$; zero traction is applied at the surface of the cavity and the outer surfaces specified by $x = -0.5$ and $y = -0.5$. All other surfaces are treated as the symmetric surfaces.

The simulated displacements along the z-direction, u_z, at point $A(0,0,0.5)$ at different discretizations are listed in Table 2. Due to the lack of the analytical solution in this case, numerical solution,$u_z = -3.1265 \mu m$, obtained from the finite element analysis using the commercial software ANSYS with 33132 SOLID95 elements and 47752 nodes is used as the reference value for the error calculation. Again, the accuracy of the pFFT accelerated BEM and its linear convergence are demonstrated.

6 Mechanical characterization of porous solids

The effective elastic properties of porous materials can be obtained based on the principle of energy equivalence; that is, by equating the total strain energy of a representative sample of the porous material subject to a specific loading to the total strain energy of the same sample subject to the same loading but made of an effective homogeneous material, of which the material properties are to be found.

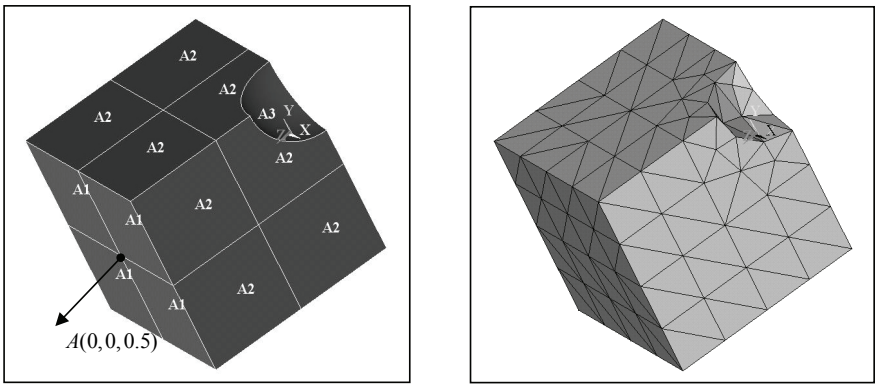

(a) Simulation model (b) Surface mesh with 220 panels

Figure 7: Model and surface discretization of a cube with a spherical cavity.

Table 2: Illustration of the convergence and efficiency of the fast pFFT BEM and its comparison with the direct BEM

Method		Number of panels			
		220	852	3350	13366
pFFT BEM	memory (MB)	8	41	168	599
	time (s)	6	14	157	503
	$u_z(A)\,\mu m$	-3.168	-3.151	-3.134	-3.131
	error	1.33%	0.78%	0.24%	0.14%
Direct BEM	memory (MB)	22	235		
	time (s)	13	182		
	$u_z(A)\,\mu m$	-3.160	-3.148		
	error	1.07%	0.69%		

The loading can be either a specified displacement or a specified traction boundary condition, which yields an upper bound or a lower bound for the effective Young's, bulk and shear moduli respectively. For Poisson's ratio, an upper bound is obtained if a traction boundary is prescribed while a lower bound is obtained by applying a displacement loading.

Both effective Young's modulus E and Poisson's ratio can be calculated by applying a uniaxial traction or a uniaxial displacement to the sample. To determine the effective bulk modulus, a uniform normal traction $\sigma^0\mathbf{n}$ or a linear displacement field corresponding to an isotropic strain ε^0 is applied on the outer surfaces of a

representative sample. Based on the "energy equivalence", the two bounds of the bulk modulus can be obtained as $K^L = \frac{\sigma^0 V}{\sum_{j=1}^{M} (\mathbf{n}\cdot\mathbf{u}A)_j}$ and $K^U = \frac{\sum_{j=1}^{M} (\mathbf{T}\cdot\mathbf{x}A)_j}{9\varepsilon^0 V}$, where K^L and K^U denote the lower and the upper bounds, respectively, M is the total number of elements on the outer surfaces, $(\mathbf{n},\mathrm{A},\mathbf{x},\mathbf{u},\mathbf{T})_j$ represent the outward unit normal vector, the area, the centroid, the displacement and the traction of the j-th element, and V is the volume of the representative sample. Similarly, the effective shear modulus is obtained as $G^L = \frac{\tau^2 V}{\sum_{j=1}^{M} (\mathbf{T}\cdot\mathbf{u}A)_j}$ or $G^U = \frac{\sum_{j=1}^{M} (\mathbf{T}\cdot\mathbf{x}A)_j}{4\gamma^2 V}$, corresponding to the loading conditions of $T_1 = \tau n_2, T_2 = \tau n_1, T_3 = 0$ and $u_1 = \gamma x_2, u_2 = \gamma x_1, u_3 = 0$, respectively. In this work, both bounds are obtained and the average value of the two bounds serves as the simulated effective property.

Due to the randomly distributed pores, the sample size and the statistical fluctuation may have strong influence on the calculated properties. In order to obtain accurate predictions of the properties, the sample size when compared with the pore size must be sufficiently large so that the influence of sample size on the effective properties is minimum. Fig. 8 plots the normalized effective Young's modulus E/E_mas a function of the normalized sample size L/r, where r is the radius of the spherical pores. The Young's modulus and Poisson's ratio of the matrix material in this calculation are chosen to be $E_m = 70GPa$ and $\nu_m = 0.25$. It is observed that when the normalized sample size is larger than 10, the Young's modulus starts to converge and becomes independent of the sample size. Hence, a sample size of 12 or larger is employed in the calculations presented in this paper. To minimize the influence of the statistical fluctuations, the material properties are calculated by taking the average of the values obtained from several different realizations of the same material; that is, samples with different distributions of pores but with the same porosity, pore size and shape.

In the following subsections, effective elastic properties of various porous solids with randomly but homogeneously distributed ellipsoidal pores are presented. Of particular interest are the effects of the porosity and pore shape on the effective elastic properties. A surface mesh with a total of 83842 triangular elements is employed in all the calculations presented. This value is determined from a convergence study. Table 3 presents the normalized effective Young's moduli obtained from two sets of meshes and four samples; each contains 64 spherical pores and has a volume porosity of 0.2. Clearly a mesh with 83842 elements is sufficiently fine for the purpose of obtaining effective linear properties.

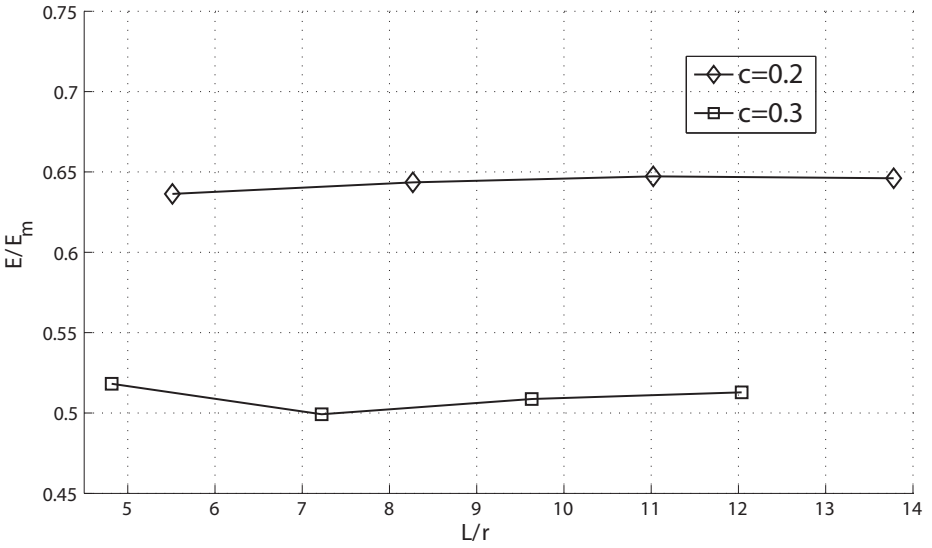

Figure 8: Normalized Young's modulus as a function of the normalized sample size.

Table 3: Convergence Study

E/E_m	83842 elements	191814 elements	Relative error (%)
Sample 1	0.6441	0.6400	0.6406
Sample 2	0.6398	0.6357	0.6449
Sample 3	0.6429	0.6387	0.6576
Sample 4	0.6437	0.6396	0.6410
Average	0.6426	0.6385	0.6421

6.1 Porosity effect

The simulated effective properties of porous samples with different porosities are plotted in Fig.9. The error bars indicate the range of variations caused by different realizations and the dots represent the average values obtained from different realizations. As expected, the effective Young's modulus, shear modulus and bulk modulus corresponding to the case with a prescribed traction boundary condition are lower than that of the case when a displacement boundary condition is prescribed. On the contrary, Poisson's ratio obtained from cases with a traction boundary condition is larger than that from cases with a displacement boundary condition. The differences between the two bounds at different porosities are listed in Table 4. It is observed that the difference increases with the increased porosity.

All three elastic moduli decrease with the increasing porosity and exhibit a slightly non-linear dependence on the porosity. The dependence of Poisson's ratio on the porosity is however much weaker and is subject to a larger fluctuation. Despite the variation, a steady reduction in Poisson's ratio is observed before the porosity reaches 0.35. It seems that Poisson's ratio starts to increase with the porosity after 0.35.

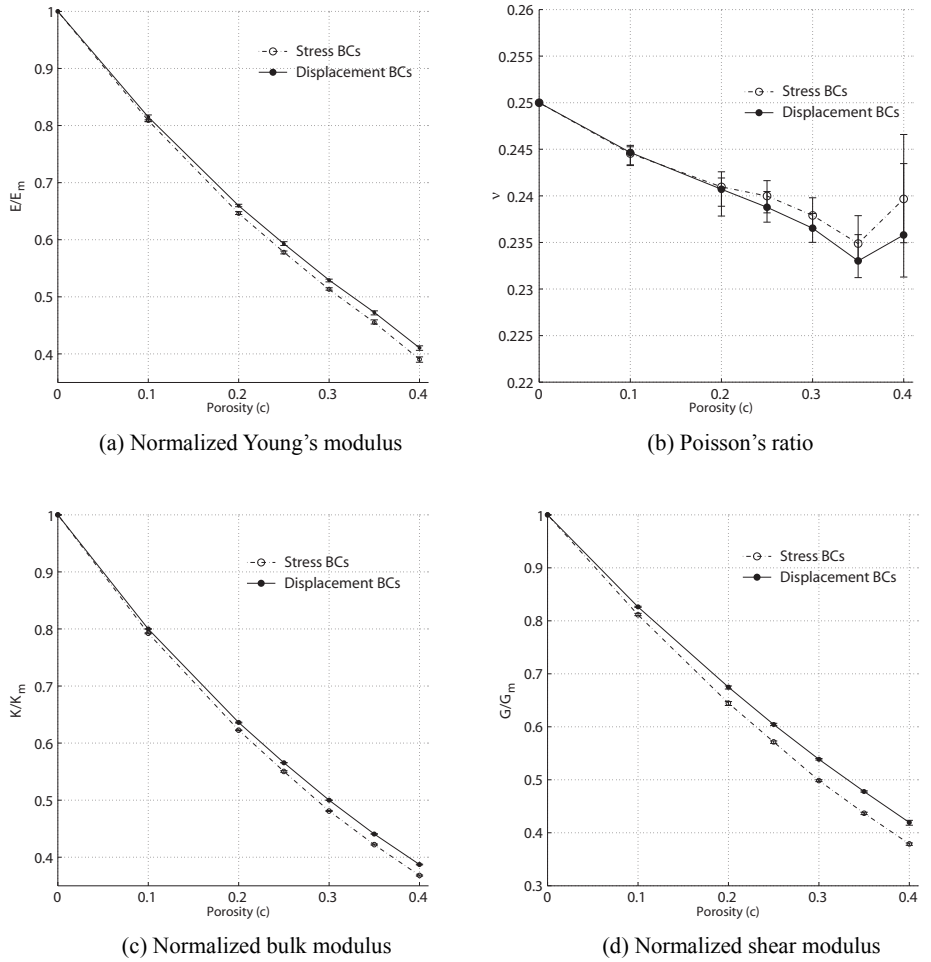

(a) Normalized Young's modulus

(b) Poisson's ratio

(c) Normalized bulk modulus

(d) Normalized shear modulus

Figure 9: Simulated effective elastic properties of a porous solid with spherical pores as functions of its porosity.

Table 4: Relative differences of elastic properties between the two bounds

Relative difference	c=0.1	c=0.2	c=0.25	c=0.3	c=0.35	c=0.4
$\Delta E/E_m(\%)$	0.79	2.09	2.54	3.21	3.87	5.14
$\Delta v(\%)$	0.05	0.10	0.51	0.58	0.79	1.61
$\Delta K/K_m(\%)$	0.95	2.17	2.76	3.95	4.41	5.19
$\Delta G/G_m(\%)$	1.84	4.67	5.76	7.98	9.41	10.69

6.2 Shape effect

The effects of pore shape on the Young's modulus and Poisson's ratio are studied by varying the radius along one semi-principal axis of the ellipsoid while keeping the radii along the other two semi-principal axes fixed, i.e., by varying the aspect ratio of the ellipsoidal pores, λ, defined as the ratio of a and b, where a and b are the radii of the ellipsoid along two principal axes. The generation of randomly distributed ellipsoidal pores with a specific λ is described in Section 2. The orientation of the ellipsoids is random but uniformly distributed. At each λ, four samples with the same porosity are constructed and modeled. The simulated Young's modulus as a function of the aspect ratios is plotted in Fig.10, which demonstrates a decreasing Young's modulus with the decreased λ. Such a trend is consistent with that observed in He, Lim and Lim (2008), in which the effective Young's moduli were simulated for cubes containing uniformly distributed ellipsoidal voids of different aspect ratio. It was found that the stiffness of the cube varied with the aspect ratio and the orientation of the voids. When the angle between the major axis of the ellipsoid and the z-axis is smaller than 45°, the stiffness increases with the increased aspect ratio. It decreases with the increased aspect ratio when the angle is larger than 45°. However, when compared with the case of spherical pores, the amount of change in the stiffness is not equal in the two cases. The increase in the stiffness when the angle is smaller than 45° is larger than the amount of the reduction in the stiffness when the angle is larger than 45°. Therefore, in our case, even when the angle is uniformly distributed, the effective Young's modulus of the cube with randomly distributed ellipsoidal pores increases with the increased aspect ratio. Due to the large variations, the effect of pore shape on Poisson's ratio is inconclusive.

6.3 Comparison between theoretical models and numerical simulations

It is of interest to compare the numerical predictions of effective elastic properties of porous solids with those obtained from various theoretical models. Due to the various assumptions employed in the theoretical models, numerical characterization of realistic materials is a viable approach for the evaluation of the performance

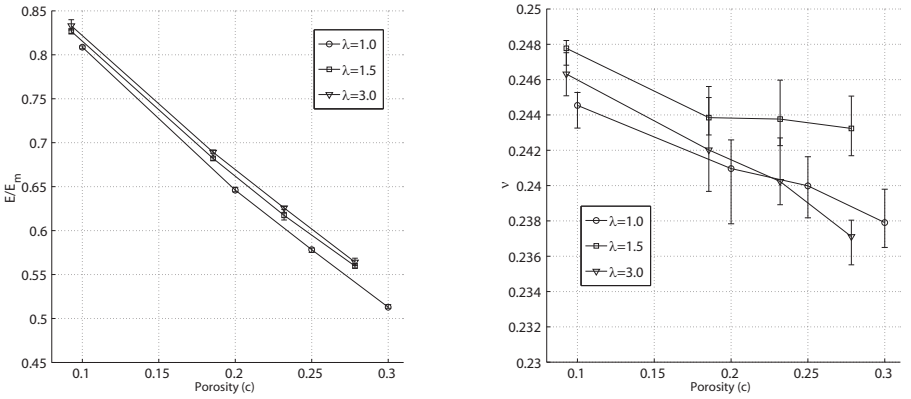

(a) normalized Young's modulus (b) Poisson's ratio

Figure 10: Simulated Young's modulus and Poisson ratio of porous solids with different ellipsoidal pores.

of these models. In Fig. 11, Young's modulus, Poisson's ratio, bulk and shear moduli of porous solids with 125 randomly but homogeneously distributed spherical pores obtained from numerical simulations and various theoretical models are presented. Again, the numerical values are the averages of the upper and lower bounds. Among the four theoretical schemes, the performances of Mori-Tanaka's method and the generalized self-consistent method (GSCM) are comparable in the prediction of the effective Young's, bulk and shear moduli with the GSCM's performance being slightly better. Both models give much better predictions than the other two methods. The self-consistent method yields the worst predictions of all properties. All methods except Mori-Tanaka's method do not produce good predictions of the effective Poisson's ratio. The good performance of Mori-Tanaka's scheme in the present examples is not surprising as this scheme is derived for materials with randomly distributed ellipsoidal inclusions. As illustrated in Benveniste (1987), the inclusion/pore interaction is accounted in a similar way as that in the GSCM which explains to a certain extent the similar performance of the two methods.

7 Summary

A 3D precorrected-FFT accelerated BEM approach is developed for the linear elastic analysis of porous solids with randomly distributed pores of arbitrary shape and size. This approach enables the direct simulation of porous solids with large porosity; hence accurate predictions of elastic behavior of realistic porous solids can be produced. The developed BEM code is validated using two examples in which

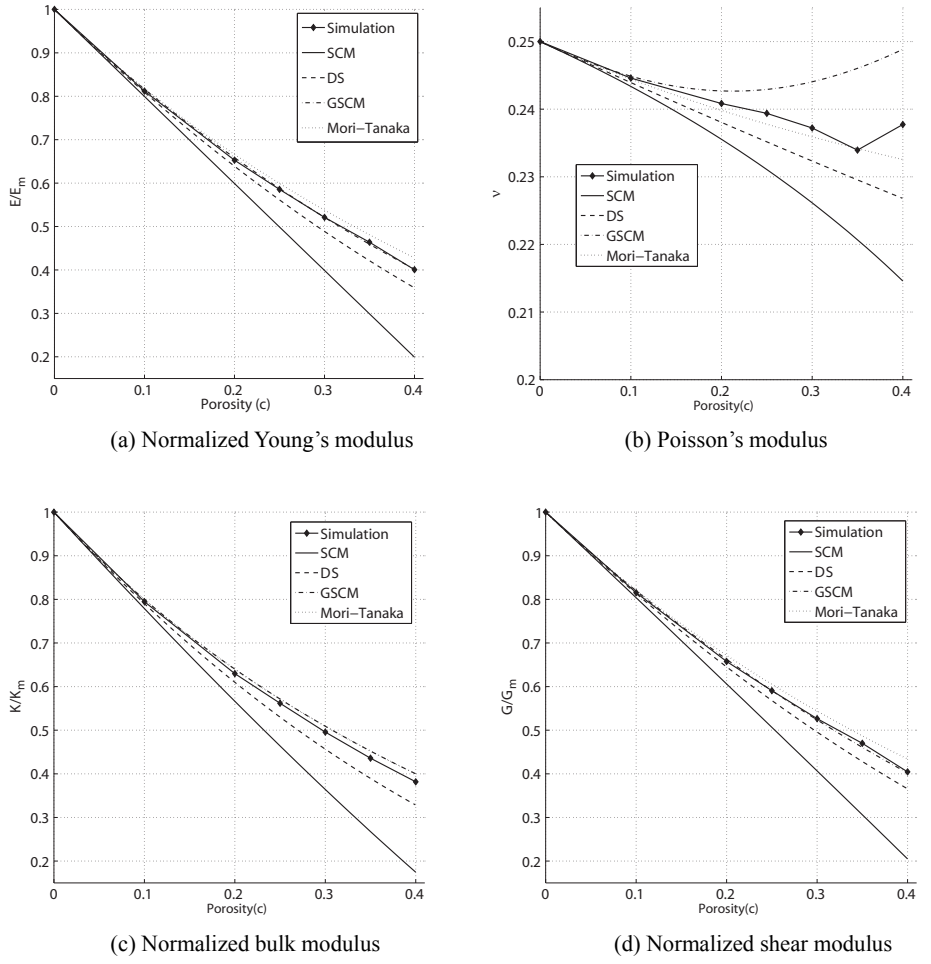

(a) Normalized Young's modulus

(b) Poisson's modulus

(c) Normalized bulk modulus

(d) Normalized shear modulus

Figure 11: Comparison between theoretical schemes and numerical simulations

the analytical solution and the numerical solution obtained by finite element calculations are used for comparison. The accuracy and the efficiency of the BEM approach have been demonstrated in both examples. As an application of the developed fast BEM approach, the Young's, shear and bulk moduli and Poisson's ratio of porous solids with spherical pores of different porosities are calculated. Both upper and lower bounds are obtained and the average values of the two bounds are used as the numerical predictions of the elastic properties. The largest porosity simulated in the present work is 0.4. This value is largely limited by the methods for model generation. The effects of porosity and pore shape on elastic properties are

investigated using numerical simulations. Despite being macroscopically isotropic, the Young's modulus of materials with ellipsoidal pores depends on the aspect ratio of the ellipsoids.

The developed approach is also employed to evaluate the performances of various theoretical schemes for the predictions of effective material properties of composite/porous materials. Overall, both the generalized self-consistent method and Mori-Tanaka's method perform quite well compared to the self-consistent method and the differential scheme by Norris. The generalized self-consistent method gives the best approximations to the three elastic moduli, while Mori-Tanaka method agrees well with the numerical value of Poisson's ratio.

Acknowledgement: This research has been supported by Hong Kong Research Grants Council under Competitive Earmarked Research Grant 621607.

References

Aimi, A.; Diligenti, M.; Lunardini, F.; Salvadori, A. (2003): A new application of the panel clustering method for 3D SGBEM. *CMES: Computer Modeling in Engineering and Sciences*, 4(1): 31-50.

Aoki, S.; Amaya, K.; Urago, M.; Nakayama, A. (2004): Fast multipole boundary element analysis of corrosion problems. *CMES: Computer Modeling in Engineering and Sciences*, 6(2): 123-132.

Banerjee, P. K. (1994): Boundary element methods in engineering. McGraw-Hill book Company.

Bebendorf, M.; Rjasanow, S. (2003): Adaptive low-rank approximation of collocation matrices. *Computing*, 70(1): 1-24.

Becker, A. A. (1992): The boundary element method in engineering. McGraw-Hill Book Company.

Benveniste, Y. (1987): A new approach to the application of Mori-Tanaka's theory in composite materials. *Mechanics of Materials*, 6(2): 147-157.

Benveniste, Y. (2008): Revisiting the generalized self-consistent scheme in composites: Clarification of some aspects and a new formulation. *Journal of the Mechanics and Physics of Solids*, 56(10): 2984-3002.

Brancati, A.; Aliabadi, M. H.; Benedetti, I. (2009):Hierarchical adaptive cross approximation GMRES Technique for solution of acoustic problems using the boundary element method, *CMES: Computer Modeling in Engineering & Sciences*, 43(2), 149-172.

Budiansky, B. (1965): On the elastic moduli of some heterogeneous materials.

Journal of the Mechanics and Physics of Solids, 13(4): 223-227.

Chen, J. T.; Hong, H. K. (1999): Review of dual boundary element methods with emphasis on hypersingular integrals and divergent series. *Applied Mechanics Reviews*, 52(1): 17-32.

Chew, W. C.; Song ,J. M.; Cui, T. J.; Velamparambil, S.; Hastriter, M. L.; Hu, B. (2004): Review of large scale computing in electromagnetics with fast integral equation solvers. *CMES: Computer Modeling in Engineering and Sciences*, 5(4): 361-372.

Christensen, R. M. (1998): Two theoretical elasticity micromechanics models. *Journal of Elasticity*, 50(1): 15-25.

Christensen, R. M.; Lo, K. H. (1979): Solutions for effective shear properties in three phase sphere and cylinder models. *Journal of the Mechanics and Physics of Solids*, 27(4): 315-330.

Criado, R.; Ortiz, J. E.; Mantič, V.; Gray, L. J.; París, E. (2007): Boundary element analysis of three-dimensional exponentially graded isotropic elastic solids. *CMES: Computer Modeling in Engineering and Sciences*, 22(2): 151-164.

Cruse, T. A. (1969): Numerical solutions in three dimensional elastostatics. *International Journal of Solids and Structures*, 5(12): 1259-1274.

Day, A. R.; Snyder, K. A.; Garboczi, E. J.; Thorpe, M. F. (1992): The elastic moduli of a sheet containing circular holes. *Journal of the Mechanics and Physics of Solids*, 40(5): 1031-1051.

Ding, J.; Ye, W. (2004): A fast integral approach for drag force calculation due to oscillatory slip Stokes flows. *International Journal for Numerical Methods in Engineering*, 60(9): 1535-1567.

Dominguez, J.; Ariza, M. P.; Gallego, R. (2000): Flux and traction boundary elements without hypersingular or strongly singular integrals. *International Journal for Numerical Methods in Engineering*, 48(1): 111-135.

Frangi, A.; Gioia, A. D. (2005): Multipole BEM for the evaluation of damping forces on MEMS. *Computational Mechanics*, 37(1): 24-31.

Gao, X. W.; Yang, K.; Wang, J. (2008): An adaptive element subdivision technique for evaluation of various 2D singular boundary integrals. *Engineering Analysis with Boundary Elements*, 32(8): 692-696.

Gatt, J. M.; Monerie, Y.; Laux, D.; Baron, D. (2005): Elastic behavior of porous ceramics: Application to nuclear fuel materials. *Journal of Nuclear Materials*, 336(2-3): 145-155.

Greengard, L.; Rokhlin, V. (1997): A new version of the fast multipole method for the Laplace equation in three dimensions. *Acta Numer.*, 6: 229-269.

Gusev, A. A. (1997): Representative volume element size for elastic composites: A numerical study. *Journal of the Mechanics and Physics of Solids*, 45(9): 1449-1459.

Hackbusch, W.; Nowak, Z. P. (1989): On the fast matrix multiplication in the boundary element method by panel clustering. *Numer. Math*. 54: 463-491.

Han, Z. D.; Atluri, S. N. (2007): A systematic approach for the development of weakly-singular BIEs. *CMES: Computer Modeling in Engineering and Sciences*, 21(1): 41-52.

Hashin, Z. (1962): The elastic moduli of heterogeneous materials. *Journal of Applied Mechanics, Transactions ASME*.

Hashin, Z.; Shtrikman, S. (1963): A variational approach to the theory of the elastic behavior of multiphase materials. J. Mech. Phys. Solids, 13: 213-222.

He, X. F.; Lim, K. M.; Lim, S. P. (2008): Fast BEM solvers for 3D Poisson-type equations. *CMES: Computer Modeling in Engineering and Sciences*, 35(1): 21-48.

He, X. F.; Lim, K. M.; Lim, S. P. (2008): A fast elastostatic solver based on fast Fourier transform on multipoles (FFTM). *International Journal for Numerical Methods in Engineering*, 76(8): 1231-1249.

Hill, R. (1965): A self-consistent mechanics of composite materials. *Journal of the Mechanics and Physics of Solids*, 13(4): 213-222.

Hu, N.; Wang, B.; Tan, G. W.; Yao, Z. H.; Yuan, W. F. (2000): Effective elastic properties of 2-D solids with circular holes: Numerical simulations. *Composites Science and Technology*, 60(9): 1811-1823.

Hwang, K. C.; Huang, Y., (1999). Constitutive relationship of solids. Tsinghua University Press, Beijing.

Kari, S.; Berger, H.; Rodriguez-Ramos, R.; Gabbert, U. (2007): Computational evaluation of effective material properties of composites reinforced by randomly distributed spherical particles. *Composite Structures*, 77(2): 223-231.

Kari, S.; Berger, H.; Rodriguez-Ramos, R.; Gabbert, U. (2007): Numerical evaluation of effective material properties of transversely randomly distributed unidirectional piezoelectric fiber composites. *Journal of Intelligent Material Systems and Structures*, 18(4): 361-372.

Karlis, G. F.; Tsinopoulos, S. V.; Polyzos, D.; Beskos, D. E. (2008): 2D and 3D boundary element analysis of mode-I cracks in gradient elasticity. *CMES: Computer Modeling in Engineering and Sciences*, 26(3): 189-207.

La Mantia, M.; Dabnichki, P. (2008): Unsteady 3D boundary element method for oscillating wing. *CMES: Computer Modeling in Engineering and Sciences*, 33(2): 131-153.

Li, J.; Wu, J. M.; Yu, D. H. (2009): Generalized extrapolation for computation of hypersingular integrals in boundary element methods. *CMES: Computer Modeling in Engineering and Sciences*, 42(2): 151-175.

Liu, Y. (2006): A new fast multipole boundary element method for solving large-scale two-dimensional elastostatic problems. *International Journal for Numerical Methods in Engineering*, 65(6): 863-881.

Liu, Y.; Nishimura, N.; Otani, Y. (2005): Large-scale modeling of carbon-nanotube composites by a fast multipole boundary element method. *Computational Materials Science*, 34(2): 173-187.

Liu, Y. J. (2000): On the simple-solution method and non-singular nature of the BIE/BEM - a review and some new results. *Engineering Analysis with Boundary Elements*, 24(10): 789-795.

Liu, Y. J.; Nishimura, N.; Otani, Y.; Takahashi, T.; Chen, X. L.; Munakata, H. (2005): A fast boundary element method for the analysis of fiber-reinforced composites based on a rigid-inclusion model. *Journal of Applied Mechanics, Transactions ASME*, 72(1): 115-128.

Lu, M. W.; Luo, X. F., (1997). Fundamental elasticity theory. Tsinghua University Press, Beijing.

Lu, Z.; Huang, Z.; Wang, R. (1995): Determination of effective moduli for foam plastics based on three phase spheroidal model. *Acta Mechanica Solida Sinica*, 8(4): 294-302.

Masters, N.; Ye, W. (2004): Fast BEM solution for coupled 3D electrostatic and linear elastic problems. *Engineering Analysis with Boundary Elements*, 28(9): 1175-1186.

Mori, T.; Tanaka, K. (1973): Average stress in matrix and average elastic energy of materials with misfitting inclusions. *Acta Metallurgica*, 21(5): 571-574.

Nagarajan, A.; Mukherjee, S. (1993): A mapping method for numerical evaluation of two-dimensional integrals with 1/r singularity. *Computational Mechanics*, 12(1-2): 19-26.

Norris, A. N. (1985): A differential scheme for the effective moduli of composites. *Mechanics of Materials*, 4(1): 1-16.

Ong, E. T.; Lim, K. M.; Lee, K. H.; Lee, H. P. (2003): A fast algorithm for three-dimensional potential fields calculation: Fast Fourier Transform on Multipoles. *Journal of Computational Physics*, 192(1): 244-261.

Owatsiriwong, A.; Phansri, B.; Park, K. H. (2008): A cell-less BEM formulation for 2D and 3D elastoplastic problems using particular integrals. *CMES: Computer Modeling in Engineering and Sciences*, 31(1): 37-59.

Phillips, J. R.; White, J. K. (1997): A Precorrected-FFT method for electrostatic analysis of complicated 3-d structures. *IEEE Transactions on Computer-Aided Design of Integrated Circuits and Systems*, 16(10): 1059-1072.

Qian, Z. Y.; Han, Z. D.; Atluri, S. N. (2004): Directly derived non-hyper-singular boundary integral equations for acoustic problems; their solution through Petrov-Galerkin schemes. *CMES: Computer Modeling in Engineering and Sciences*, 5(6): 541-562.

Qian, Z. Y.; Han, Z. D.; Ufimtsev, P.; Atluri, S. N. (2004): Non-hyper-singular boundary integral equations for acoustic problems, implemented by the collocation-based boundary element method. *CMES: Computer Modeling in Engineering and Sciences*, 6(2): 133-144.

Rintoul, M. D.; Torquato, S. (1997): Reconstruction of the structure of dispersions. *Journal of Colloid and Interface Science*, 186(2): 467-476.

Roberts, A. P.; Garboczi, E. J. (2000): Elastic properties of model porous ceramics. *Journal of the American Ceramic Society*, 83(12): 3041-3048.

Saad, Y.; Schultz, M. (1986): GMRES: A generalized minimal residual algorithm for solving symmetric linear systems. *SIAM Journal on Scientific and Statistical Computing*, 7: 856-869.

Sanz, J. A.; Solis, M.; Dominguez, J. (2007): Hypersingular BEM for piezoelectric solids: Formulation and applications for fracture mechanics. *CMES: Computer Modeling in Engineering and Sciences*, 17(3): 215-229.

Scuderi, L. (2008): On the computation of nearly singular integrals in 3D BEM collocation. *International Journal for Numerical Methods in Engineering*, 74(11): 1733-1770.

Segurado, J.; Gonzalez, C.; Llorca, J. (2003): A numerical investigation of the effect of particle clustering on the mechanical properties of composites. *Acta Materialia*, 51(8): 2355-2369.

Segurado, J.; Llorca, J. (2002): A numerical approximation to the elastic properties of sphere-reinforced composites. *Journal of the Mechanics and Physics of Solids*, 50(10): 2107-2121.

Simone, A. E.; Gibson, L. J. (1998): Effects of solid distribution on the stiffness and strength of metallic foams. *Acta Materialia*, 46(6): 2139-2150.

Soares, J. D.; Vinagre, M. P. (2008): Numerical computation of electromagnetic fields by the time-domain boundary element method and the complex variable method. *CMES: Computer Modeling in Engineering and Sciences*, 25(1): 1-8.

Tan, C. L.; Shiah, Y. C.; Lin, C. W. (2009): Stress analysis of 3D generally anisotropic elastic solids using the boundary element method. *CMES: Computer*

Modeling in Engineering and Sciences, 41(3): 195-214.

Wang, H. T.; Hall, G.; Yu, S. Y.; Yao, Z. H. (2008): Numerical simulation of graphite properties using X-ray tomography and fast multipole boundary element method. *CMES: Computer Modeling in Engineering and Sciences*, 37(2):153-174.

Wang, H. T.; Yao, Z. H. (2005): A new fast multipole boundary element method for large scale analysis of mechanical properties in 3D particle-reinforced composites. *CMES: Computer Modeling in Engineering and Sciences*, 7(1): 85-96.

Wang, H. T.; Yao, Z. H. (2008): A rigid-fiber-based boundary element model for strength simulation of carbon nanotube reinforced composites. *CMES: Computer Modeling in Engineering and Sciences*, 29(1): 1-13.

Wang, H. T.; Yu, S. Y. (2008): Large-scale numerical simulation of mechanical and thermal properties of nuclear graphite using a microstructure-based model. *Nuclear Engineering and Design*, 238(12): 3203-3207.

Wang, W.; Wang, J.; Kim, M. S. (2001): An algebraic condition for the separation of two ellipsoids. *Computer Aided Geometric Design*, 18(6): 531-539.

Yan, Z. Y.; Cui, F. S.; Hung, K. C. (2005): Investigation on the normal derivative equation of helmholtz integral equation in acoustics. *CMES: Computer Modeling in Engineering and Sciences*, 7(1): 97-106.

Yan, Z. Y.; Hung, K. C.; Zheng, H. (2003): Solving the hypersingular boundary integral equation in three-dimensional acoustics using a regularization relationship. *Journal of the Acoustical Society of America*, 113(5): 2674-2683.

Yang, S. A. (2004): An integral equation approach to three-dimensional acoustic radiation and scattering problems. *Journal of the Acoustical Society of America*, 116(3): 1372-1380.

Yao, Z.; Kong, F.; Zheng, X. (2003): Simulation of 2D elastic bodies with randomly distributed circular inclusions using the BEM. *Electronic Journal of Boundary Elements*, 1(2): 270-282.

Ye, W. (2008): A new transformation technique for evaluating nearly singular integrals. *Computational Mechanics*, 42(3): 457-466.

Ye, W.; Wang, X.; Hemmert, W.; Freeman, D.; White, J. (2003): Air damping in lateral oscillating micro resonators: A numerical and experimental study. *Journal of Microelectromechanical Systems*, 12(5): 1-10.

Zozulya, V. V. (2009): Variational formulation and nonsmooth optimization algorithms in elastostatic contact problems for cracked body. *CMES: Computer Modeling in Engineering and Sciences*, 42(3): 187-215.